

Heat-pipe Earth

William B. Moore^{1,2} & A. Alexander G. Webb³

The heat transport and lithospheric dynamics of early Earth are currently explained by plate tectonic and vertical tectonic models, but these do not offer a global synthesis consistent with the geologic record. Here we use numerical simulations and comparison with the geologic record to explore a heat-pipe model in which volcanism dominates surface heat transport. These simulations indicate that a cold and thick lithosphere developed as a result of frequent volcanic eruptions that advected surface materials downwards. Declining heat sources over time led to an abrupt transition to plate tectonics. Consistent with model predictions, the geologic record shows rapid volcanic resurfacing, contractional deformation, a low geothermal gradient across the bulk of the lithosphere and a rapid decrease in heat-pipe volcanism after initiation of plate tectonics. The heat-pipe Earth model therefore offers a coherent geodynamic framework in which to explore the evolution of our planet before the onset of plate tectonics.

The lithospheric dynamics of terrestrial planets is driven by the transport of heat from the interior to the surface¹. Terrestrial bodies with low heat flows (for example Mars ($<20 \text{ mW m}^{-2}$; ref. 2) and the Moon (12 mW m^{-2} ; ref. 3)) lose heat largely by conduction across a single-plate lithosphere, whereas Earth's heat transport (global mean flux¹, 65 mW m^{-2}) is dominated by plate tectonics. Early in Earth's history, radiogenic heat production was three to five times greater than at present⁴, and there were additional contributions from tidal heating by a receding Moon and loss of accretionary heat. Whether or not plate tectonics operates under these conditions is uncertain geodynamically^{5–9}, but plate tectonic processes such as subduction and arc accretion are often invoked to explain the geologic and geochemical features of Archaean rocks^{10–12}.

An example of a terrestrial body with a higher surface heat flow than modern Earth is Jupiter's moon Io. Rather than losing heat by more vigorous plate tectonics, Io instead transports about 40 times Earth's heat flux¹³ (2.5 W m^{-2}) from the interior to the surface through volcanism. This mode of planetary heat transport is called the heat-pipe mode^{14,15} after the localized channels through which melt brings heat to the surface. Heat pipes are conduits that transfer heat and material from the base of the lithosphere to the surface by means of buoyant ascent (for example the lithospheric plumbing atop a mantle plume). When heat pipes become the dominant heat transport mechanism of a planet, the effects on the lithosphere are both surprising and profound.

Geodynamic models of heat-pipe Earth

We explore the consequences of the heat-pipe mode for early Earth using simplified models of mantle convection with melt generation and extraction. The temperature field snapshots shown in Fig. 1 result from numerical solutions to the equations of mass, energy and momentum transport in the mantle¹⁶ as internal heating and cooling at the surface drive convective motions (for details of the modelling approach and parameter definitions, see Methods Summary). These two-dimensional models have a strongly temperature-dependent, Newtonian rheology that results in a single-plate, rigid lid at the surface. Melting and melt transport are modelled in as simple a fashion as possible while preserving the effect of this process on the heat transport and dynamics of the lithosphere. Melt is generated whenever the mantle exceeds a simple linearly pressure-dependent solidus¹⁷ and is immediately extracted

to the surface, and the column in which the melt was produced is advected downwards to conserve mass (Fig. 1, inset). Once at the surface, the melt is assumed to lose its latent and sensible heat (which is tracked as volcanic heat flow) instantly and to return to the imposed surface boundary temperature of 15°C . Although this is a simplification of the process of melt generation and eruption, it captures the basic physics in a manner that allows us to see clearly the effects of heat pipes on the lithosphere.

The internal heating and surface heat flow both increase by a factor of ten from top to bottom in Fig. 1. Increased internal heat production causes the temperature of the mantle to increase slightly and the thickness of the cold lid to increase significantly. A thick, cold lithosphere develops because volcanic material deposited at the surface buries old flows, resulting in a descending 'conveyor belt' of material

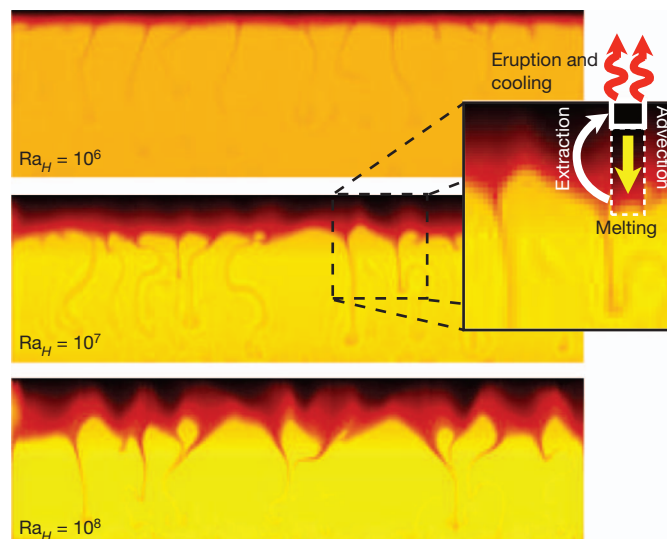


Figure 1 | Snapshots of the temperature field for two-dimensional models of mantle convection. The internal-heating Rayleigh number, Ra_H , is different in each panel. The inset illustrates the operation of the heat pipe: melt is extracting to the surface, where it cools, and cold lithosphere is advected downwards to conserve mass.

¹Department of Atmospheric and Planetary Sciences, Hampton University, Hampton, Virginia 23668, USA. ²National Institute of Aerospace, Hampton, Virginia 23666, USA. ³Department of Geology and Geophysics, Louisiana State University, Baton Rouge, Louisiana 70803, USA.

that advects the cold surface temperature to great depths (Fig. 1, inset). Because heat-pipe volcanism is global, the constant resurfacing and downward advection causes compression as the surface rocks are forced radially inward, resulting in uplift, exhumation and shortening. This process of contraction is observed on Io¹⁸, which has many mountains more than 10 km high that are clearly fault-bounded tectonic uplifts.

We explore the effect of heat pipes on the thermal structure of the lithosphere in more detail by constructing steady-state solutions of the energy equation with a term that accounts for the downward advection at a velocity v (ref. 14):

$$\frac{k}{\rho c_p} \frac{d^2 T}{dz^2} = v \frac{dT}{dz} - \frac{H}{\rho c_p} \quad (1)$$

where k is the thermal conductivity ($4 \text{ W m}^{-1} \text{ K}^{-1}$), ρ is the density ($3,000 \text{ kg m}^{-3}$), c_p is the specific heat capacity at constant pressure ($1,000 \text{ J kg}^{-1} \text{ K}^{-1}$) and H is the volumetric heat production rate (10^{-7} W m^{-3} at 4 Gyr ago). Material reaching the base of the lithosphere, defined by the dry peridotite solidus¹⁷, melts and returns to the surface through heat pipes. In Fig. 2, we plot solutions for three different lithospheric thicknesses (120, 150 and 180 km) and three different advection rates (0.1, 1 and 10 mm yr^{-1}). Rapid downward advection ($>0.5 \text{ mm yr}^{-1}$) brings materials to high pressures before they are significantly heated. Thermal equilibrium through heat pipes in early Earth requires a global average resurfacing by flows of $1\text{--}2 \text{ mm yr}^{-1}$ (whereas the rate on Io is 10 mm yr^{-1}). Partial melting and intra-lithospheric differentiation may also occur, resulting in more evolved lithologies erupting and intruding back up through the stack. The intrusions would locally modify the temperature structure by delivering heat to shallower regions. When advection slows or stops, the lithosphere re-warms as geotherms relax towards the conductive profile.

In addition to altering the thickness and thermal structure of the lithosphere, heat pipes influence the stress distribution as shown in Fig. 3, where we plot the maximum stress observed in the lithosphere as a function of the internal heating rate. Volcanic heat pipes are the dominant heat transport mechanism at high heat production rates (Fig. 3a, solid line), reflecting higher mantle temperatures and increased rates of melting. The maximum stress experienced in the lithosphere (Fig. 3b) has a distinct minimum that coincides with the crossover between heat-pipe and conductive heat transport. This behaviour occurs because heat pipes remove buoyancy from the actively convecting boundary layer at the top of the mantle, reducing convective stresses, while at the same time producing a thicker lithosphere. Therefore, active

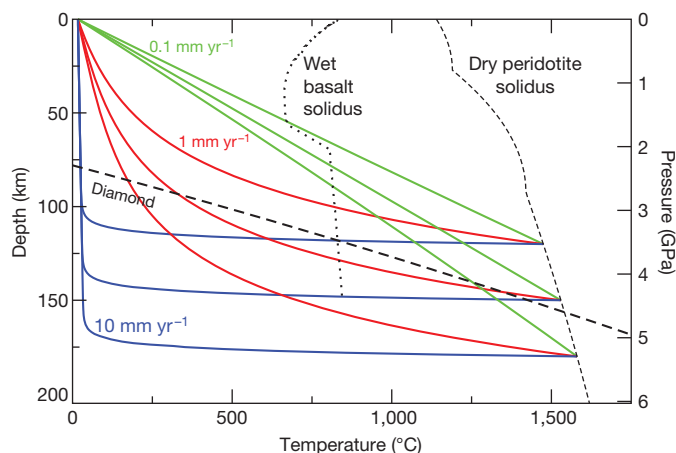


Figure 2 | Temperature as a function of depth in lithosphere. Three downward advection rates (0.1 , 1 and 10 mm yr^{-1}) are shown, each for three lithosphere thicknesses (120, 150 and 180 km). Also shown are the stability limit of diamond³⁹ (thick dashed), the wet basalt solidus¹¹ (dotted) and the dry peridotite solidus¹⁷ (thin dashed), which is chosen to define the base of the lithosphere.

heat pipes would lead to a very different lithospheric stress regime in early Earth than at present, as indicated in Fig. 3b.

We also performed simulations to identify the transition out of the heat-pipe mode of heat transport (Fig. 4). For these cases, we modelled the finite strength of the lithosphere by using a yield stress (Methods Summary). The transition is caused by the decline in heat sources (red line), which gradually causes the volcanic heat flow (cyan line) to decrease. At about the time the volcanic heat flow becomes small compared with the conductive heat flow (black line), the plate breaks and the entire lithosphere is replaced in a sudden overturn. This is an artefact of our two-dimensional approach; in three dimensions, the overturn would replace only portions of the lithosphere. Breaking occurs because the peak lithospheric stress increases with declining heat production, eventually overcoming the strength of the lithosphere and allowing the negative buoyancy of the cold material to drive rapid flow. There is a rapid decrease in volcanism (cyan) after lithospheric overturn.

Geologic evidence for heat-pipe Earth

The heat-pipe Earth hypothesis and simulations supply predictions for early Earth's development: rapid volcanic resurfacing, a low geothermal gradient across the bulk of the lithosphere, contractional deformation (with minor extensional deformation in restricted settings such as grabens atop rising diapirs) and a rapid decrease in heat-pipe volcanism after initiation of plate tectonics. Preserved heat-pipe rocks would be broadly representative of the single-plate lithosphere. Here we review the geologic record of early Earth and compare it with these predictions and those of existing models. We focus on the period before ~ 3.2 Gyr ago because interpretations of diverse data suggest that plate tectonics began at that time: isotopic records in zircons indicate a pronounced decrease in crustal growth rate¹⁹, inclusion assemblages of kimberlite-hosted diamonds shift from exclusively peridotitic to eclogitic as well as peridotitic²⁰, and a Wilson cycle that occurred 3.2–3.1 Gyr ago has been identified²¹.

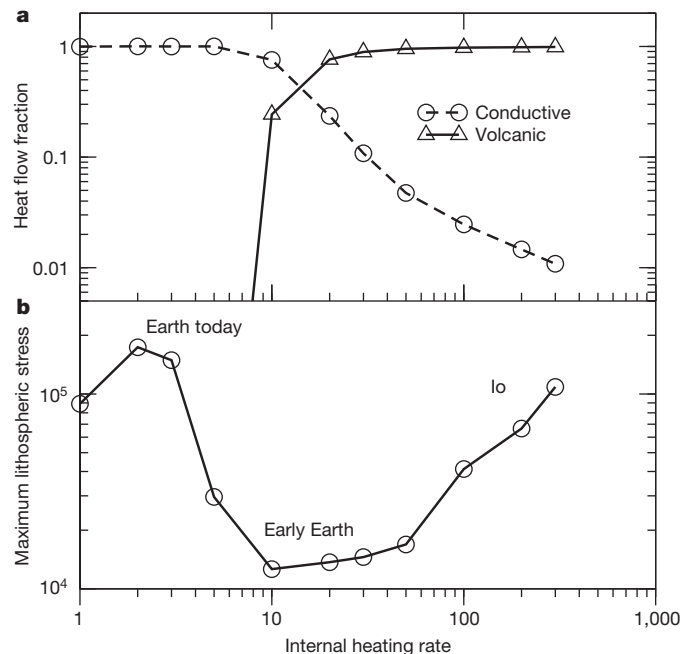


Figure 3 | Heat flow contributions and dimensionless maximum lithospheric stress as functions of the dimensionless internal heating rate ($\alpha HD^2/k$). a, Heat flow; b, maximum lithospheric stress. Volcanic heat-pipe transport dominates at higher internal heating rates. This causes a marked decrease in lithospheric stress. At very high heating rates (Io), lithospheric thickness variations lead to larger stresses. All quantities are long-term averages over quasi-steady conditions.

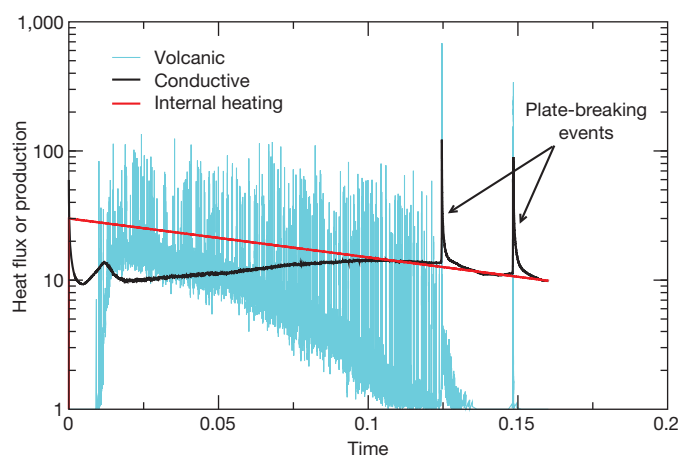


Figure 4 | Internal heat production, surface conductive heat transport and surface volcanic heat transport as functions of time in a model with a finite yield stress. The heat production has been converted into an equivalent surface flux by integrating over depth. The time is made dimensionless using the thermal diffusion timescale. Plate-breaking events are identified at times 0.125 and 0.15.

The best-preserved rock records from before 3.2 Gyr ago are from the Barberton (South Africa) and Pilbara (Australia) greenstone belts, which extend back to 3.55 and 3.53 Gyr ago, respectively^{22,23}. Before ~3.2 Gyr ago, both belts experienced similar geologic histories. Mafic and ultramafic volcanic rocks were erupted in alternating subaerial and marine settings and occur as thick sequences: ~10 km thick at Barberton and ~20 km at Pilbara^{22–24}. Minor chemical sediments, locally derived clastic sediments and felsic tuffs are interspersed in the mafic piles and commonly occur below unconformities^{22,23,25}. Deposition of volcanic and sedimentary rocks was episodic and semiregular. For example, at Pilbara eight cycles, each ~15 Myr long, have been identified, with the five deepest cycles forming a >12-km-thick section deposited over 100 Myr (ref. 25). Tonalite–trondhjemite–granodiorite (TTG) plutons comprise about half of the >3.2-Gyr-old rocks exposed across both sites and were intruded in several 30–60-Myr-long episodes spanning the 300-Myr history of each belt^{23,26}. The TTG rocks represent melts of two sources: pre-existing TTG and hydrated mafic rocks²⁶. Melts of hydrated mafic rocks were generated at pressures and temperatures ranging from 1.5 GPa and ~1,000 °C to ≥3.0 GPa and ~1,200 °C (refs 11, 26), suggesting heat flows of <50 to 80 mW m⁻². The upper limit of the pressure estimates is poorly constrained because the melt reactions have little to no pressure dependence¹¹. The more deeply sourced melts show evidence of interaction with ultramafic material during melt ascent²⁶.

Emplacement of the TTG plutons as rising diapirs developed a dome-and-syncline regional structural pattern, with the volcanic sequences deformed into downwelled synclinal troughs^{25,27}. Internal deformation associated with this downwelling may thin the volcanic sequences by 50% or more²⁷, causing estimated eruption rates to be lower limits. Apart from the diapir deformation, both belts are essentially undeformed until ~3.2 Gyr ago. At this time, rifting, arc development and accretion occurred at Pilbara²¹, whereas deformation and metamorphism associated with either collisional tectonics²² or rapid diapir emplacement²⁷ occurred at Barberton. These are the last medium–high-temperature events experienced by most portions of both belts^{22,28}.

Other than at Barberton and Pilbara, the >3.2 Gyr-old rock record is limited to gneiss complexes as old as ~4.03 Gyr ago²⁹. Some of the complexes show >3.2-Gyr-old migmatization, suggesting deformation before that time³⁰. The 3.85–3.55-Gyr-old Itsaq gneiss complex (Greenland) is broadly representative of these gneisses and preserves the best-defined deformation record. It experienced high-grade metamorphism, granite production and terrane juxtaposition along a series of mylonitic shear zones over a 100-Myr period^{10,30} (~3.65–3.55 Gyr

ago). In addition to granite, gneiss protolith lithologies here include all Barberton and Pilbara lithologies as well as limited slices of ≥3.65-Gyr-old peridotite^{10,31}. More than 95% of the rocks are metamorphosed felsic plutons with igneous crystallization ages spanning the age of the complex^{10,30}. Two suites of felsic rocks are derived from hydrated mafic rocks both above and below ~45-km depth, and from remelted TTG^{10,32}. Like at Barberton and Pilbara, maximum melting depths are unconstrained¹¹. Clastic metasediments are dominantly derived from the mafic or ultramafic volcanics, with minor detrital input from the other lithologies³³. All detrital material is restricted to narrow age ranges just slightly older than the timing of sedimentation³³.

Although the rock record ends at ~4 Gyr ago, detrital zircon grains provide evidence of earlier times: the oldest zircons from the Jack Hills locality (Australia) are nearly 4.4 Gyr old. Hafnium, oxygen and lead isotope information from zircon grains have been used to demonstrate that a population of Jack Hills zircon grains ranging in age from ~4.3 to 3.9 Gyr were sourced from melts of weathered material that formed in the presence of water^{34,35}, that a population of Jack Hills zircon grains grew in a ~4.1-Gyr-old felsic pluton which itself resulted from remelting of 4.36–4.30-Gyr-old TTG³⁶, and that the sources of TTGs have not changed during the past 4.3 Gyr (ref. 12). Also, a population of Jack Hills zircon grains ranging in age from ~4.25 to 3.2 Gyr features variable Th/U ratios and inclusions of ultrahigh-pressure metamorphic diamonds³⁷. The diamonds show a wide range of carbon isotope ratios, even in the same zircon, indicating a diversity of carbon sources that most probably reflects surface processes³⁸. Therefore, the diamonds probably represent former surface material, and they crystallized at depths of >100 km and were subsequently included in igneous zircon^{37,38}.

Comparison of the >3.2-Gyr-old geologic record with the predictions of heat-pipe Earth reveals that a wide range of structural, kinematic, petrologic and isotopic data are consistent with the operation of heat pipes. The long duration of rapid volcanic resurfacing observed at Barberton and Pilbara matches the main surface prediction of the heat-pipe hypothesis. The thickness and age limits of the volcanic sequences allow estimation of downward advection rates: approximately 0.03, 0.07 and 0.12 mm yr⁻¹ for the Barberton, Pilbara and lower-Pilbara sections, respectively. These rates must be considered minima because the preserved volcanic sequences contain unconformities and occur in the thinned limbs of downwelled synclines. Similarly, the restricted age range of clastic sediment source material at Itsaq might indicate rapid volcanic resurfacing³³. In general, we speculate that interpretations applied to the Barberton and Pilbara greenstone belts may be similarly applicable to Itsaq because of the broad correspondence in protolith lithologies.

Downward advection accounts for the low geothermal gradients implied by melting conditions. Felsic volcanics and TTG plutons may all be sourced from a downwards-advecting lithosphere comprising TTG and mafic or ultramafic materials. Melting of the shallow lithosphere to produce low-pressure TTG melts probably occurs in response to thermal perturbations caused by the rise of hot, deeply sourced TTG melts. The possible rapid TTG diapir emplacement and the onset of rifting ~3.2 Gyr ago are consistent with the rewarming of the lithosphere associated with both the end of heat-pipe cooling and the initiation of plate tectonics. Heat-pipe cooling would have to be significantly diminished after ~3.2 Gyr ago, because the Barberton and Pilbara rocks did not experience significant subsequent burial. This is consistent with the abrupt drop in volcanism seen in Fig. 4.

Within the context of the heat-pipe hypothesis, deformation such as the ~3.65–3.55-Gyr-old protracted tectonothermal event at Greenland might be interpreted as either development of a subduction zone¹⁰ or a long-lived reverse-fault duplex system. The first option may be possible because our simulations suggest that heat-pipe mode would continue to contribute to cooling after a subduction event (Fig. 4). Nonetheless, the second option seems more likely given the abrupt decrease in heat-pipe volcanism after ~3.2 Gyr ago. Also, peridotite has been interpreted

as oceanic crust in the first hypothesis^{10,31}, but these rocks may represent ultramafic plutonic rocks or deeply buried lavas.

Jack Hills zircon constraints demonstrate that TTGs as old as ~4.4 Gyr were generated by melting and remelting of material that was previously weathered at the surface^{12,34–36}. This is consistent with the ~4.0–3.2-Gyr-old rock record, suggesting that analogous geodynamic interpretations apply at least as far back as ~4.4 Gyr ago. The inclusion of diamond with likely surface signatures in similar zircons is interpreted in the heat-pipe Earth context to indicate that the lithospheric conveyor belt was operating to a depth of >100 km ~4.25 Gyr ago, and plausibly until 3.2 Gyr ago, which is consistent with the cold, thick lithosphere produced in heat-pipe Earth (Figs 1 and 2). Also shown in Fig. 2 are melting curves for wet basalt¹¹ and dry peridotite¹⁷, and the phase boundary for diamond³⁹. Because the only means of exhuming these diamonds is the ascent of TTG plutons, some of these plutons must be sourced within the diamond stability field. This is consistent with the intersection of the wet basalt solidus and the heat-pipe geotherm (for example the red lines in Fig. 2).

Previous explanations of the >3.2-Gyr-old geologic record can be loosely divided into protoplate tectonic models and vertical tectonics models⁴⁰. Plate tectonic models involve horizontal plate motion, with spreading ridges and subduction zones to create and reprocess lithosphere⁴¹. Vertical tectonic models posit lithospheric evolution through sub- and intra-lithospheric diapirism, associated downwelling and volcanism, and basal delamination. The central challenge of the early-Earth record for plate tectonic models is that important products of plate tectonics, many of which have high preservation potential (for example paired metamorphic belts and passive margins), are absent⁴⁰. In contrast, the record contains features not readily explained by proposed vertical tectonic processes. Namely, terrane juxtaposition such as seen at Greenland, where peridotite slices may be interpreted as ophiolites, has been explained only by incorporating horizontal motion akin to plate motion^{40,42}. As a result of including such kinematics, these models face similar problems as plate tectonic models.

The geology of Barberton and Pilbara illustrates the difficulties inherent in previous models. These sites preserve no deformation for >300 Myr, with the exception of diapiric deformation. Current plate and vertical tectonic models explain this geology in terms of prolonged mantle plume volcanism^{23,27}. However, all such models involve significant horizontal translation of lithosphere, which presents two problems. First, it would be highly unusual in a plate tectonic regime for two plumes, or two successions of plumes, to remain fixed at both sites for >300 Myr. Second, there is no evidence of horizontal motion in the record. Cooling by means of heat pipes does not have similar problems because it features semi-continuous volcanism and minor horizontal contraction globally.

A new model for early Earth tectonics

The heat-pipe hypothesis implies that early Earth's lithospheric dynamics was very different from that today. Similar to Jupiter's volcanically active moon Io, early Earth transported heat in the heat-pipe mode, with melt rising through narrow conduits and downward advection of the lithosphere beneath newer flows. The lithosphere is thickened and the geotherm is depressed by the advection (Figs 1 and 2). Lithospheric stresses are reduced by a combination of thickening and the loss, through the heat pipes, of buoyancy from the convective thermal boundary layer at the top of the mantle (Fig. 3). These model predictions are all consistent with the main features of the >3.2-Gyr-old geologic record, which is dominated by deeply sourced, high-melt-fraction volcanic rocks that have interacted with water and sedimentary products from the surface. The transition from heat pipes to plate tectonics has also been modelled, showing a rapid switch between modes (Fig. 4) that matches the geologic record at Barberton and Pilbara. Heat-pipe Earth provides a coherent dynamic framework for the understanding of planetary evolution from initial crystallization of the lithosphere atop the magma ocean to the onset of plate tectonics.

METHODS SUMMARY

The calculations presented here use the STAG3D code¹⁶ to solve the equations of mass, momentum and energy conservation for infinite-Prandtl-number Boussinesq flow in a 4×1 , two-dimensional domain spanning the depth of the mantle. The system is made dimensionless by using the mantle depth, D , as the length scale, D^2/κ as the time scale (κ , thermal diffusivity) and D^2H/k as the temperature scale, resulting in the definition¹ of the internal-heating Rayleigh number $Ra_H = \alpha \rho g H D^5 / k \eta \kappa$ with thermal expansivity α , gravitational acceleration g and viscosity η . For all simulations presented here, $Ra_H/H = 10^6$.

The Newtonian, exponentially temperature-dependent rheology has a total viscosity contrast that ranges from 10^4 to 10^7 as H varies from 1 to 300. The computational grid is 256×64 or 512×128 depending on the Rayleigh number.

For the time-dependent simulation with a finite yield stress, $H = 30$ and an effective viscosity, η_{eff} , was specified to incorporate a yield stress σ_y , as follows⁶:

$$\sigma_{ij} = 2 \frac{\sigma_y^2 \eta}{\sigma_y^2 + \eta^2 \dot{\epsilon}^2} \dot{\epsilon}_{ij} \equiv 2 \eta_{\text{eff}} \dot{\epsilon}_{ij}$$

Here σ_{ij} and $\dot{\epsilon}_{ij}$ are the stress and strain rate components, respectively, and $\dot{\epsilon}^2$ is the square of the second invariant of the strain tensor. The value of the yield stress was chosen to intersect the maximum lithospheric stress curve in the lower panel of Fig. 3.

The one-dimensional models of equation (1) have constant temperature boundary conditions applied at the surface and at an arbitrary depth identified as the base of the lithosphere.

Received 24 March; accepted 12 July 2013.

- Turcotte, D. L. & Schubert, G. *Geodynamics* 1–17, 2nd edn (Cambridge Univ. Press, 2002).
- McGovern, P. J. *et al.* Correction to “Localized gravity/topography admittance and correlation spectra on Mars: implications for regional and global evolution”. *J. Geophys. Res.* **109**, E07007 (2004).
- Warren, P. H. & Rasmussen, K. L. Megaregolith insulation, internal temperatures, and bulk Uranium content of the Moon. *J. Geophys. Res.* **92**, 3453–3465 (1987).
- Franck, S. Evolution of the global mean heat flow over 4.6 Gyr. *Tectonophysics* **291**, 9–18 (1998).
- Davies, G. F. Gravitational depletion of the early Earth's upper mantle and the viability of early plate tectonics. *Earth Planet. Sci. Lett.* **243**, 376–382 (2006).
- Korenaga, J. Thermal evolution with a hydrating mantle and the initiation of plate tectonics in the early Earth. *J. Geophys. Res. Solid Earth* **116**, B12403 (2011).
- O'Neill, C. J., Lenardic, A., Moresi, L., Torsvik, T. H. & Lee, C.-T. A. Episodic pre-Cambrian subduction. *Earth Planet. Sci. Lett.* **262**, 552–562 (2007).
- van Hunen, J. & van den Berg, A. P. Plate tectonics on the early Earth: limitations imposed by strength and buoyancy of subducted lithosphere. *Lithos* **103**, 217–235 (2008).
- van Hunen, J., & Moyer, J.-F. Archean subduction: fact or fiction? *Annu. Rev. Earth Planet. Sci.* **40**, 195–219 (2012).
- Nutman, A. P., Friend, C. R. L., Horie, K. & Hikada, H. in *Earth's Oldest Rocks* (eds Van Kranendonk, M. J., Smithies, R. H. & Bennett, V. C.) 187–218 (Elsevier, 2007).
- Moyer, J.-F. The composite Archean grey gneisses: petrological significance, and evidence for a non-unique tectonic setting for Archean crustal growth. *Lithos* **123**, 21–36 (2011).
- Guitreau, M., Blichert-Toft, J., Martin, H., Mojszisz, S. J. & Albareda, F. Hafnium isotope evidence from Archean granitic rocks for deep-mantle origin of continental crust. *Earth Planet. Sci. Lett.* **337–338**, 211–223 (2012).
- Veeder, G. J., Matson, G. J., Johnson, T. V., Davies, A. G. & Blaney, D. L. The polar contribution to the heat flow of Io. *Icarus* **169**, 264–270 (2004).
- O'Reilly, T. C. & Davies, G. F. Magma transport of heat on Io: a mechanism allowing a thick lithosphere. *Geophys. Res. Lett.* **8**, 313–316 (1981).
- Breuer, D., & Moore, W. B. in *Treatise on Geophysics* Vol. 10 (ed. Schubert, G.) 299–341 (Elsevier, 2007).
- Tackley, P. J. Modelling compressible mantle convection with large viscosity contrasts in a three-dimensional spherical shell using the yin-yang grid. *Phys. Earth Planet. Inter.* **171**, 7–18 (2008).
- Takahashi, E. Melting of a dry peridotite KLB-1 up to 14 GPa: implications on the origin of peridotitic upper mantle. *J. Geophys. Res.* **91**, 9367–9385 (1986).
- Schenk, P. M. & Bulmer, M. H. Origin of mountains on Io by thrust faulting and large-scale mass movements. *Science* **279**, 1514–1517 (1998).
- Dhuime, B., Hawkesworth, C. J., Cawood, P. A. & Storey, C. D. A change in the geodynamics of continental growth 3 billion years ago. *Science* **335**, 1334–1336 (2012).
- Shirey, S. B. & Richardson, S. H. Start of the Wilson cycle at 3 Ga shown by diamonds from subcontinental mantle. *Science* **333**, 434–436 (2011).
- Pease, V., Percival, J., Smithies, R. H., Stevens, G. & Van Kranendonk, M. in *When Did Plate Tectonics Begin On Planet Earth?* (eds Condie, K. C. & Pease, V.) 199–228 (The Geological Society of America, 2008).
- Lowe, D. R. & Byerly, G. R. in *Earth's Oldest Rocks* (eds Van Kranendonk, M. J., Smithies, R. H. & Bennett, V. C.) 481–526 (Elsevier, 2007).
- Van Kranendonk, M. J., Smithies, R. H., Hickman, A. H. & Champion, D. C. in *Earth's Oldest Rocks* (eds Van Kranendonk, M. J., Smithies, R. H. & Bennett, V. C.) 307–337 (Elsevier, 2007).

24. Stiegler, M. T., Lowe, D. R. & Byerly, G. R. Fragmentation and dispersal of komatiitic pyroclasts in the 3.5–3.2 Ga Onverwacht Group, Barberton greenstone belt, South Africa. *Geol. Soc. Am. Bull.* **123**, 1112–1126 (2011).
25. Hickman, A. H. & Van Kranendonk, M. J. in *The Precambrian Earth: Tempos and Events* (eds Eriksson, P. G., Altermann, W., Nelson, D. R., Mueller, W. U. & Catuneanu, O.) 54–75 (Elsevier, 2004).
26. Moyen, J.-F., Stevens, G., Kisters, A. F. M. & Belcher, R. W. in *Earth's Oldest Rocks* (eds Van Kranendonk, M. J., Smithies, R. H. & Bennett, V. C.) 607–667 (Elsevier, 2007).
27. Van Kranendonk, M. J. Cool greenstone drips and the role of partial convective overturn in Barberton greenstone belt evolution. *J. Afr. Earth Sci.* **60**, 346–352 (2011).
28. Zegers, T. E., Wijbrans, J. R. & White, S. H. $^{40}\text{Ar}/^{39}\text{Ar}$ age constraints on tectonothermal events in the Shaw area of the eastern Pilbara granite-greenstone terrain (W. Australia): 700 Ma of Archaean tectonic evolution. *Tectonophysics* **311**, 45–81 (1999).
29. Bowring, S. A. & Williams, I. S. Priscoan (4.00–4.03 Ga) orthogneisses from northwestern Canada. *Contrib. Mineral. Petrol.* **134**, 3–16 (1999).
30. Friend, C. R. L. & Nutman, A. P. Complex 3670–3500 Ma orogenic episodes superimposed on juvenile crust accreted between 3850–3690 Ma, Itsaq Gneiss Complex, southern West Greenland. *J. Geol.* **113**, 375–397 (2005).
31. Friend, C. R. L., Bennett, V. C. & Nutman, A. P. Abyssal peridotites >3,800 Ma from southern West Greenland: field relationships, petrology, geochronology, whole-rock and mineral chemistry of dunite and harzburgite inclusions in the Itsaq Gneiss Complex. *Contrib. Mineral. Petrol.* **143**, 71–92 (2002).
32. Hoffmann, J. E. *et al.* Mechanisms of Archean crust formation inferred from high-precision HFSE systematics in TTGs. *Geochim. Cosmochim. Acta* **75**, 4157–4178 (2011).
33. Kamber, B. S., Whitehouse, M. J., Bolhar, R. & Moorbath, S. Volcanic resurfacing and the early terrestrial crust: zircon U-Pb and REE constraints from the Isua Greenstone Belt, southern West Greenland. *Earth Planet. Sci. Lett.* **240**, 276–290 (2005).
34. Mojzsis, S. J., Harrison, T. M. & Pidgeon, R. T. Oxygen-isotope evidence from ancient zircons for liquid water at the Earth's surface 4,300 Myr ago. *Nature* **409**, 178–181 (2001).
35. Wilde, S. A., Valley, J. W., Peck, W. H. & Graham, C. M. Evidence from detrital zircons for the existence of continental crust and oceans on the Earth 4.4 Gyr ago. *Nature* **409**, 175–178 (2001).
36. Blichert-Toft, J. & Alverède, F. Hafnium isotopes in Jack Hills zircons and the formation of the Hadean crust. *Earth Planet. Sci. Lett.* **265**, 686–702 (2008).
37. Menneken, M., Nemchin, A. A., Geisler, T., Pidgeon, R. T. & Wilde, S. A. Hadean diamonds in zircon from Jack Hills, Western Australia. *Nature* **448**, 917–920 (2007).
38. Nemchin, A. A. *et al.* A light carbon reservoir recorded in zircon-hosted diamond from the Jack Hills. *Nature* **454**, 92–95 (2008).
39. Bundy, F. P. Pressure-temperature phase-diagram of elemental carbon. *Physica A* **156**, 169–178 (1989).
40. Stern, R. J. Modern-style plate tectonics began in Neoproterozoic time: an alternative interpretation of Earth's tectonic history. *Spec. Pap. Geol. Soc. Am.* **440**, 265–280 (2008).
41. Harrison, T. M. The Hadean crust: evidence from >4 Ga zircons. *Annu. Rev. Earth Planet. Sci.* **37**, 479–505 (2009).
42. Bédard, J. H., Harris, L. B. & Thurston, P. C. The hunting of the snArc. *Precamb. Res.* **229**, 20–48 (2013).

Acknowledgements This research has been supported by NSF Geophysics, NASA PG&G, the NASA Astrobiology Institute and a start-up fund from Louisiana State University, and has made use of the Astrophysics Data System. We thank M. Stiegler for discussions.

Author Contributions Both authors contributed to the writing of this paper. W.B.M. performed the numerical modelling and A.A.G.W. provided the review of the geologic literature.

Author Information Reprints and permissions information is available at www.nature.com/reprints. The authors declare no competing financial interests. Readers are welcome to comment on the online version of the paper. Correspondence and requests for materials should be addressed to W.B.M. (william.moore@hamptonu.edu).